NOISE GENERATED FROM AN ARRAY OF CURRENT ENERGY CONVERTERS

Erin Hafla, Charles Johnson, and Erick Johnson[1]
Montana State University
Bozeman, MT, USA

Jesse D Roberts
Sandia National Laboratories
Albuquerque, NM, USA

[1]Corresponding author: erick.johnson@montana.edu

INTRODUCTION

As new sources of anthropogenic noise, arrays of current- and wave-energy converters (CECs and WECs, respectively) will add to other man-made and natural sources in the marine environment. Regulatory constraints and environmental concerns over the sound pressure levels produced by these devices may be a hurdle to their deployment and operation. The Marine Mammal Protection Act in the USA, for example, limits disturbance and injury, where the present classification of total noise levels permissible are below 120 dB and 180 dB re 1 µPa, respectively [1]. While initial studies from individual devices are promisingly below 120 dB [2-6], alternative device designs, equipment failure, or array deployment could potentially surpass these levels. Each device type will create unique noise profiles and levels, and how those spectra change between individual deployment sites will need to be predicted (either through experiments or modeling efforts) in order to meet regulatory requirements for permitting and deployment.

Shallow water environments are likely to be louder due to increased anthropogenic and natural noise sources in a constrained space, such as from shipping traffic, breaking waves, sediment/debris transport, and environmental variability [7,8]. Few measurements from controlled experiments [2] and in-situ studies [3-5] or predictions from models [6] exist to build a conclusive understanding of the types of noise produced from these devices. The addition of new marine hydrokinetic (MHK) sources will couple to the total sound level of the system and has the potential to push that total over regulatory and environmental limits. However, dependent upon the sound pressure level (SPL) produced by individual MHK devices, their arrangement in an array, and the local site characteristics, these additions may have little contribution relative to all the sources even considering their additive nature. Sound pressure level is defined as

$$SPL = 20 \log\left(\frac{P_{RMS}}{P_{ref}}\right) \qquad 1)$$

where P_{RMS} is the root mean square of the pressure at a specific location over time and P_{ref} is a reference pressure of 1 µPa, for water. P_{RMS} can be calculated in octave or 1/3-octave bands (commonly used when the frequency content of the noise is needed, such as for biological studies) or as a broadband of all frequencies. The latter is chosen for this work and follows the definition of the NOAA Interim Sound Threshold Guidance [1]; however, a draft of updated guidelines is currently under review [9].

The modeled, or measured, SPL can then be used to understand how particular species respond [10-13]. Insonification studies of marine species detail what sounds, levels, and frequencies are impactful [10,14]. Eulerian Lagrangian-agent methods (ELAM) coupled with hydrodynamic models can provide a mechanism to statistically predict changes to behavior of marine animals or fish populations in response to particular stimuli [12,13]. Based upon the model, temporary and permanent shifts in hearing levels can then be determined [11,14]. However, these conclusions will be highly dependent upon the calculated SPL from an array of devices. Farcas *et al*. highlights the overall infancy of underwater noise modeling and integration into environmental impact assessments [15].

This work investigates the broadband noise generated from an array of CECs and how the array shape and size impact the sound environment. Extension to particular frequency bands and updated NOAA guidelines for marine mammals will be performed in a more detailed analysis to follow.

METHODOLOGY

Paracousti is a parallelized acoustic-wave propagation package developed at Sandia National Labs [16]. It solves a linearization of Cauchy's equations of motion that become the coupled set of velocity-pressure equations shown below (Equations 2 and 3).

$$\frac{\delta v_i(\boldsymbol{x},t)}{\delta t}+\frac{1}{\rho(\boldsymbol{x})}\frac{\delta p(\boldsymbol{x},t)}{\delta \boldsymbol{x}_i} = \frac{1}{\rho(\boldsymbol{x})}\left[F_i(\boldsymbol{x},t)+\frac{\delta {m_{ij}}^a(\boldsymbol{x},t)}{\delta \boldsymbol{x_j}}\right] \quad 2)$$

$$\frac{\delta p(\boldsymbol{x},t)}{\delta t}+\kappa(\boldsymbol{x})\frac{\delta v_i(\boldsymbol{x},t)}{\delta \boldsymbol{x}_i} = -\frac{1}{3}\frac{\delta {m_{ii}}^s(\boldsymbol{x},t)}{\delta t} \quad 3)$$

where $v_i(\boldsymbol{x},t)$ and $p(\boldsymbol{x},t)$ are the perturbations of particle velocity (m/s) and pressure (Pa), $\rho(\boldsymbol{x})$ is the material density (kg/m^3), and $\kappa(\boldsymbol{x})$ is the material bulk modulus (Pa) of the medium. The right-hand side terms in Equations 2 and 3 are body source terms: $F_i(\boldsymbol{x},t)$ is the force density vector (N/m^3), ${m_{ij}}^a(\boldsymbol{x},t)$ is the anti-symmetric portion of the moment density tensor and ${m_{ij}}^s(\boldsymbol{x},t)$ is the trace of the symmetric portion of the moment density tensor (N/m^2). A summation is implied by the repeated indices of the tensor. The velocity-pressure equations are discretized with the finite-difference method and are second-order accurate in time and fourth-order accurate in space. Paracousti can simulate sound propagation within realistic 3-D earth-, atmosphere-, and hydro-acoustic domains simultaneously, and allows for 3-D variations in medium densities, acoustic sound speeds, and bathymetry. The code currently assumes that the densities and sound speeds are fixed in time over the duration of a simulation. While the steady assumptions can be relaxed, it assumed that a ±0.3% change in sound speed (~4.5 m/s variation of flow in a tidal straight relative to a 1500 m/s sound speed) can be neglected for these preliminary investigations.

Monopole sources within Paracousti are defined as

$$\sum \frac{A}{4\pi c^2}(1-\cos(2\pi\omega t)) \quad 4)$$

where ω is the frequency (Hz) of the source corresponding to a particular pressure amplitude A (Pa) at 1 m from the source, t is the present simulation time (s), and c is the average system sound speed (m/s). The profile is summed over all relevant/desired frequencies. This offset cosine, as opposed to a simple sinusoid, limits the amount of numerical noise introduced when taking time-derivatives of the source at the first time step.

In comparison, both the normal mode and parabolic equation (PE) methods are solved in the frequency domain, based upon the 3-D Helmholtz equations. The normal mode method involves solving a depth-dependent equation and constructing an acoustic field by determining the contributions of each mode, weighted in accordance to the source depth. Normal modes are limited for deep water applications where high frequencies (>1 kHz) are involved. PE techniques are applied to range-dependent propagation problems with an assumed outgoing cylindrical wave solution, but are limited with respect to shallow water systems with high frequencies. Both are well suited for low frequency systems in both 1-D and 2/3-D solutions [17]. While both of these solution methods have a longstanding history within underwater acoustics, the time-dependent, velocity-pressure equations were chosen for their flexibility in domain and its properties, source profile(s), number of sources, and solution of the particle perturbations, which are being shown to have implications in fish health [18,19].

A 2-D, two-layered waveguide is used to begin this investigation. The domain is 200 m in depth and 3500 m in range, where the top half space (the first 100 meters in depth) is water with a sound speed of 1500 m/s and density of 1000 kg/m^3. The bottom half space (100-200 m depth) has a sound speed of 1800 m/s and density of 1800 kg/m^3. These values are representative of a standard 'hard bottom' modeling case [17]; however, without a reasonable estimate of porosity, the classification of the soil can chance. A value of porosity was not used for this model. The top surface has an imposed pressure-free boundary condition, which is a good approximation for the water-air interface and reflections back into the water domain. The bottom and sides of the domain utilize the convolutional perfectly-matched layer (CPML) boundary condition and absorbs nearly all of the energy that leaves the system [20]. A grid spacing of 1 m and a timestep of 0.2 ms is used.

Three CEC array configurations (shown in Figure **1**) and four inter-device spacings are investigated, where the array spacing (AS) defines the distance between devices along the perimeter.

In addition, as devices are unlikely to remain in the same phase relative to each other over their operation, the arrays are simulated 400 times with a random phase shift applied to each device. A uniform distribution is used for this random shift, with 33 potential phase shifts allowed as a result of the timestep chosen and to have a smooth source profile. For this work, each of the sources are a continuous 150 Hz with an amplitude of 1 Pa (120 dB) meant to correspond to broadband from a 5 m diameter horizontal axis turbine [21]. Array spacings of 10, 15, 20, and 40 m (or a distance of 1, 2, 3, 7 device-diameters between blade-tips) are investigated, with 10 m corresponding to one wavelength in the water column. Spacings were chosen in order to fall within wavelength nodes instead of anticipated inter-device spacing. While these distances may be considered an extreme for device proximity in the flow direction, it falls within potential spacing for flow in the perpendicular (into the page) direction. These configurations and spacings additionally have the benefit of showcasing the trends observed. Alternative array configurations, spacings, and their interaction in complex bathymetries will be investigated in future works. The center of each array was located at a depth of 50 m and a range of 20 m in order to maintain symmetry within the water column.

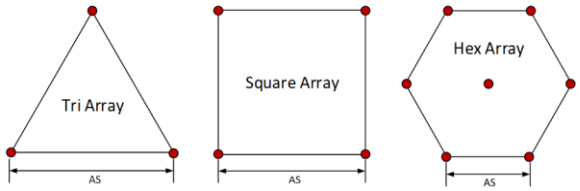

FIGURE 1. DIAGRAM OF EACH ARRAY CONFIGURATION (TRI, SQUARE, AND HEX) WITH THE ARRAY SPACING (AS) DIMENSION LABELED AND RED DOTS INDICATING SOURCE LOCATIONS

RESULTS

The first array considered is an equilateral triangle and was selected because each of the three sources maintain an equal distance from each other. Results for a depth-averaged SPL in the water column of all 400 trials for the equilateral triangle are shown in Figure 2. Each line represents one of each of the 400 trials.

The results of SPL in Figure 2 for the triangular array show some initial trends. Firstly, there appears to be a banding of SPLs that narrows as the array spacing is increased. This banding appears to be fairly constant after a few hundred meters, where the spreading transitions from purely spherical to a partially-cylindrical spread, with energy still being lost to the bed. This correlation makes sense because as the array spacing increases, the strength of sound interference between successive devices decreases due to propagation loss. An array that is closely spaced will interfere with waves of higher amplitude profiles than that of an array that is spaced further apart, where the propagating amplitude is allowed to decay much further before interacting with those from additional devices. Secondly, unique probability distributions of the depth-averaged SPL appear to develop based upon both the array configuration and spacing. The equilateral triangle has a distinctly bimodal probability distribution at an AS of 10 m that appears to collapse into a single mode as the spacing increases. The square and hexahedral array configurations tend toward single mode distributions regardless of the array spacing. Thirdly, and as expected, in the immediate vicinity of the array, the total SPL is larger than that of a single device. This is independent of the array configuration and its spacing. Lastly, and shown in Figure 3, the arithmetic mean of the depth-averaged SPL for all trials within each array spacing is nearly identical. Each line represents the depth-averaged SPL for each array spacing. Similar results are observed for each of the other two array configurations.

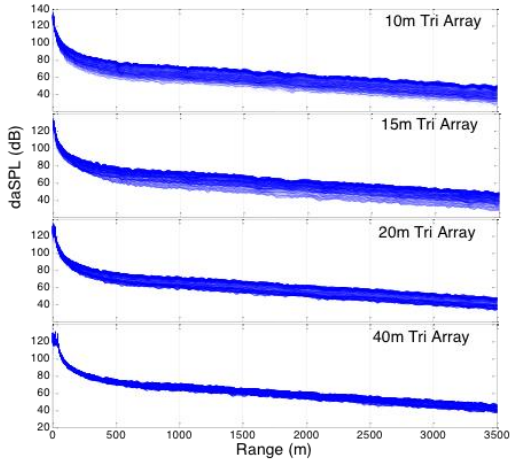

FIGURE 2. DEPTH AVERAGED SPL (dB re 1 µPa) OF WATER COLUMN FOR THE TRIANGULAR ARRAY

CONCLUSIONS

An acoustic propagation tool is used to investigate how the configuration and size of an array of current energy converts impacts the sound the entire array produces. Utilizing a random phase-shift for each of the sources results in a significant spread in potential depth-averaged, broadband SPL's propagating from an array of MHK devices. This banding decays as the devices are spaced further apart.

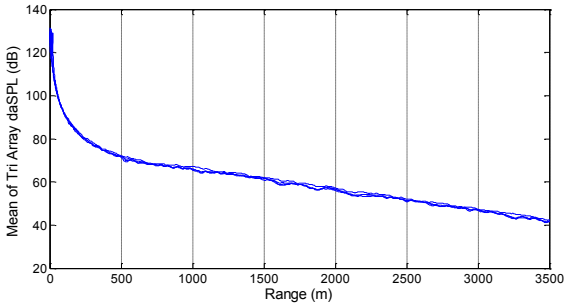

FIGURE 3. ARITHMETIC MEAN OF THE DEPTH-AVERAGED SPL (dB re 1 µPa) FOR EACH TRIANGULAR ARRAY SPACING

ACKNOWLEDGEMENTS

This work was sponsored Sandia National Laboratories' Water Power Technology department and by the Department of Energies' Wind and Water Power Technologies Office. Sandia National Laboratories is a multi-program laboratory managed and operated by Sandia Corporation, a wholly owned subsidiary of Lockheed Martin Corporation, for the U.S. Department of Energy's National Nuclear Security Administration under contract DE-AC04-94AL85000.

REFERENCES

[1] NOAA Fisheries, "Interim Sound Threshold Guidance," Available from http://www.westcoast.fisheries.noaa.gov/protected_species/marine_mammals/threshold_guidance.html. Accessed 1 March 2015.

[2] Fontaine, A. A., Straka, W.A., Meyer, R.S., and Jonson, M.L., 2013, "A 1:8.7 Scale Water Tunnel Verification & Validation Test of an Axial Flow Water Turbine," TR 13-002, Penn State University Applied Research Lab.

[3] Schmitt, P., Elsaesser, B., Coffin, M., Hood, J., Starzmann, R., 2015, "Field Testing a Full-Scale Tidal Turbine Part 3: Acoustic Characteristics," Proceedings of the 11th European Wave and Tidal Energy Conference, Nantes, France.

[4] Cruz, E., Simas, T., Kasanen, E., 2015, "Discussion of the Effects of the Underwater Noise Radiated by a Wave Energy Device – Portugal," Proceedings of the 11th European Wave and Tidal Energy Conference, Nantes, France.

[5] Polagye, B., Murphy, P., "2015, "Acoustic Characterization of a Hydrokinetic Turbine," Proceedings of the 11th European Wave and Tidal Energy Conference, Nantes, France.

[6] Jonson, M., Fahnline, J., Johnson, E., Barone, M., Fontaine, A., 2012, "Influence of Blade Solidity on Marine Hydrokinetic Turbines," Proceedings of Internoise 2012 and ASME NCAD Meeting, New York, NY, USA.

[7] Erbe, C., McCauley, R., McPherson, C., and Gavrilov, A., 2013, "Underwater noise from offshore oil production vessels," Journal of the Acoustical Society of America, vol. 133, pp. EL465-EL470.

[8] Bassett, C., 2013, "Ambient Noise in an Urbanized Tidal Channel," Doctor of Philosophy, Mechanical Engineering, University of Washington.

[9] National Oceanic and Atmospheric Administration, "DRAFT Guidance for Assessing the Effects of Anthropogenic Sound on Marine Mammal Hearing: Underwater Acoustic Threshold Levels for Onset of Permanent and Temporary Threshold Shifts", July 2015.

[10] Halvorsen, M.B., 2011, "Effects of Tidal Turbine Noise on Fish Hearing and Tissues," Environmental Effects of Marine and Hydrokinetic Energy. Prepared for the U.S. Department of Energy. Pacific Northwest National Laboratory.

[11] Popper, A.N., Hawkins, A.D., Fay, R.R., Mann, D.A., Bartol, S., Carlson, T.J., Coombs, S., Ellison, W.T., Gentry, R.L., Halvorsen, M.B., Løkkeborg, S., Rogers, P.H., Southall, B.L., Zeddies, D.G., Tavolga, W.N., 2014, ASA S3/SC1.4 TR-2014 Sound Exposure Guidelines for Fishes and Sea Turtles: A Technical Report Prepared by ANSI-Accredited Standards Committee S3/SC1 and Registered with ANSI. American National Standards Institute.

[12] Goodwin, R.A., Nestler, J.M., Anderson, J.J., Weber, L.J., and Loucks, D.P., 2006, "Forcasting 3_D fish movement behavior using a Eulerian-Lagrangian-agent method (ELAM)," Ecological Modelling, 192, pp. 197-223.

[13] Rossington, K., Benson, T., Lepper, P., and Jones, D., 2013, "Eco-hydr-acoustic modeling and its use as an EIA tool," Marine Pollution Bulletin, 75, pp. 235-243.

[14] Popper, A.N. and Fay, R.R., 2011, "Rethinking sound detection by fishes," Hearing Research, 273, pp. 25-36.

[15] Farcas, A., Thompson, P., and Merchant, N., 2016, "Underwater Noise Modelling for Environmental Impact Assessment," Environmental Impact Assessment Review, 57, 114-122.

[16] Preston, L., "Paracousti User Guide," Geophysics and Atmospheric Science Department at Sandia National Laboratories.

[17] Jensen, F., Kuperman, W., Porter, M., and Schmidt, H., 2011, "Computational Ocean

Acoustics," 2nd Edition, published by Springer Media.
[18] Hawkins, A., and Popper, A., "Effects of Noise on Fish, Fisheries, and Invertibrates in the U.S. Atlantic and Artic from Energy Industry Sound-Generating Activities," A Literature Synthesis for the U.S. Department of the Interior, Bureau of Ocean Energy Management, Feb 2012, Contract #M11PC00031.
[19] Wysocki, L., Codarin, A., Ladich, F., Picciulin, M., "Sound Pressure and Particle Acceleration Audiograms in Three Marine Fish Species from the Adriatic Sea," Journal of Acoustical Society of America, Vol. 126, No. 4, Oct 2009.
[20] Komatitsch, D. and Martin, R., "An Unsplit Convolutional Perfectly Matched Layer Improved at Grazing Incidence for the Seismic Wave Equation," *Geophysics,* 2007.
[21] Jonson, M., Johnson, E., Roberts, J., "Predicting Sound Generated from the Blades of Horizontal-Axis Water Turbines," 2015, documentation provided by Sandia National Laboratory.